Appl. Phys. A 63, 341–346 (1996)

Applied Physics A Materials Science & Processing

Reconstruction of surface topographies by scanning electron microscopy for application in fracture research

J. Stampfl[1], **S. Scherer**[2], **M. Gruber**[2], **O. Kolednik**[1]

[1]Erich-Schmid-Institut für Festkörperphysik der Österreichischen Akademie der Wissenschaften, Jahnstrasse 12, A-8700 Leoben, Austria (Fax: + 43-3842/45512-16, E-Mail: JSTAMPFL@unileoben.ac.at)
[2]Institut für Computerunterstützte Geometrie und Graphik, TU, TU-Graz, Münzgrabenstrasse 11, A-8010 Graz, Austria (E-mail: SCHERER@icg.tu-graz.ac.at)

Received: 27 November 1995/Accepted: 11 March 1996

Abstract. Stereoscopic scanning electron micrographs can be used to reconstruct the microscopic topography of material surfaces. By applying a system for automatic image processing we can obtain Digital Elevation Models (DEMs) of the investigated surface. These DEMs are used to measure the degree of deformation on metallic fracture surfaces. By modelling the deformation the amount of plastic energy that is necessary to shape the microductile fracture surface can be calculated. These values are compared with experimentally obtained results.

PACS: 07.80; 42.30; 62.00

The usability of a certain material in a mechanically loaded structure is limited by its strength. The higher the yield strength the larger are the possible loads. A problem arises when there exist precracks in the structure, e.g. caused by fatigue or corrosion. In this case the stresses concentrate at sharp notches (like cracks are) and they can become large enough to cause final failure although the average stress is below the yield stress. Especially, materials with high yield strengths have the tendency to break at low stress intensities since they are brittle and cannot diminish the stress intensities by blunting of the sharp crack tip. That is why, in addition to the strength, a second mechanical parameter (the fracture toughness) must be introduced to estimate the mechanical reliability of a structure.

One established parameter for the determination of fracture toughness is the *energy dissipation rate D* [1, 2] which is related to the amount of plastic energy that is necessary to propagate a crack. Three mechanisms contribute to the dissipation of energy during the crack extension: A certain fraction of the overall dissipated plastic energy is spent for the lateral necking of the specimen, another fraction is spent for deformations within the plastic zone outside the process zone. The third mechanism which dissipates energy is the formation of voids in the process zone. This energy term will further be called void energy. When the voids in the process zone grow and coalesce, the crack length increases.

The surface topography is reconstructed by analyzing stereoscopic Scanning Electron Microscope (SEM) images. The technique [3–8] allows the reconstruction of a 3D-object by measuring the parallaxes in two stereo images. By using a system for image processing [9, 10] we can automatically generate DEMs consisting of about 10 000 points.

The aim of this work is to estimate the amount of the void energy from analyzing the plastic deformations that led to the final fracture surface topography. Similar estimations were already done in earlier works [11, 12] by modelling the surface topography with a parabolic or ellipsoidal dimple profile. In this work, due to the use of automatic image processing, the real surface shape can be taken into account for the calculation of the deformation energy and no assumptions about the surface profile have to be made.

1 Theoretical model

1.1 Energy dissipation rate

In this section the theoretical value of the void energy obtained by analyzing the fracture surface shape will be related with experimental values of the energy dissipation rate *D*. For the calculation of the overall energy dissipation rate D_{tot} [2] from the measured values *F* (force) v_{lld} (load line displacement) and *a* (crack length) the following formula is applied:

$$D_{\mathrm{tot}} = \frac{1}{B}\frac{d}{da}(W_{\mathrm{pl}} + \Gamma) = \frac{1}{B}\frac{d}{da}(U - W_{\mathrm{el}}), \tag{1}$$

where *B* is the thickness of the specimen, Γ is the surface energy and *U* is the external work which is identical to the area below the load versus load-line displacement ($F - v_{\mathrm{lld}}$) curve. W_{el}, the elastic energy is calculated by

$$W_{\mathrm{el}} = \frac{CF_2}{2}. \tag{2}$$

C is the compliance of the sample [13] and F is the applied force. D_{tot} can now be divided into three parts, as outlined above, for the formation of voids, for subsurface deformations and for lateral necking of the specimen:

$$D_{tot} = D_{void} + D_{subsurface} + D_{ln}. \quad (3)$$

1.2 Estimation of the void energy

In [11, 14], Stüwe introduced a model to calculate the void energy (= plastic energy for the formation of the ductile fracture surface) from the shape of the fracture surface. The plastic energy $W_{pl,void}$ is given by

$$W_{pl,void} = \int_V \int_0^{\Phi} \sigma d\Phi^* \, dV, \quad (4)$$

where σ is the true flow stress and Φ the local strain. By integrating over the volume V one gets $W_{pl,void}$. V is not only the material volume but also the empty space caused by the formation of voids. Using the elementary theory of plastomechanics [15, 16] ("*plane cross sections remain plane*") one can assume that

$$\Phi = \ln \frac{A_0}{A(z)}.$$

The relief of the fracture surface is described by a series of cross sections A at the height z (Fig. 1). A will diminish from A_0 (the area of the analyzed image) at height 0 (the bottom of the deepest "valley") to zero at height h_0. The volume integral can then be replaced by an integral over z for a cross section A_0. With $D_{void} = W_{pl,void}/A_0$ we obtain

$$D_{void} = \int_0^{h_0} \sigma \frac{A(z)}{A_0} \ln \frac{A_0}{A(z)} dz. \quad (5)$$

From the DEMs of two fracture surfaces that were connected in the unbroken specimen the *misfit* of the two surfaces due to local plastic deformation can be calculated. We only have to superimpose the two DEMs and subtract the heights of the coupled points of the DEMs to obtain a void- or misfit map (see later). Coupled points are those points that were "neighbours" on the two fracture surfaces before the crack has separated them. For each pair of coupled points in the void map we know the coordinates x and y in the plane A_0 as well as the misfit height h. With this information (5) can be solved by numerical integration. Since (5) is not sensitive to very fine surface structures [11], the integral can be calculated sufficiently accurate with DEMs consisting of about 10 000 points.

The result of (5) depends on the used true flow stress σ. In [12] Poech and Fischmeister introduced a model that does not only take into account the final shape of the fracture surface but also the varying stress-strain relations during the fracture process. The derived equations lead to similar results as the simpler equations in [11] since the triaxiality imposed by the stress state in front of the crack has a strong effect only when the volume fraction of voids is close to zero. We therefore decided to use an average mean flow stress of the form $\sigma_{amf} = m\sigma_u$ [11]. σ_u is the ultimate tensile strength and m a coefficient which depends on the strain hardening exponent n of the material. In [11] a plot m versus n is given.

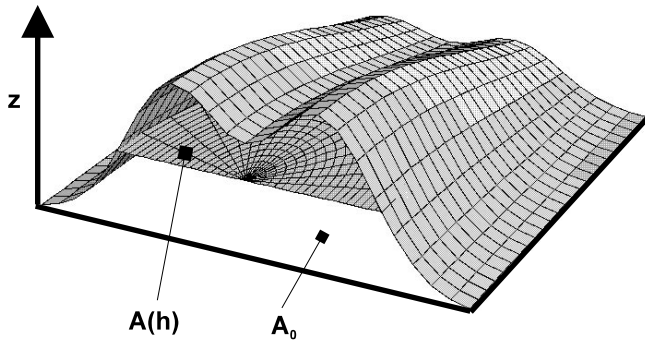

Fig. 1. The shape of the fracture surface is described by cross-sections $A(z)$

2. Stereophotogrammetry

To reconstruct the depth information from SEM images we are using stereophotogrammetric methods. The stereo images are obtained by making SEM images of the tilted and untilted specimen. The possibility of a stereoscopic examination and measurement was already used in the early days of SEM microscopy [3–5].

Stereoscopic electron microscopy provides several advantages compared with other methods for the 3D-reconstruction of microscopic objects. Since the "sensor" has no mechanical contact with the observed specimen, SEM is well suited for very rough objects like the fracture surfaces investigated in this work. Furthermore the depth of focus as well as the lateral resolution is significantly better than with optical methods. With stereoscopic SEM, lateral and vertical distances of about three millimeters down to several ten nanometers can be analyzed. Another advantage of stereoscopic SEM is that even monoscopic images contain a lot of information for the interpretation of the observed surface. In Fig. 2a we show a monoscopic SEM image of a AgCuPd-solder layer which gives already in the monoscopic view a very plastic impression of the surface topography and the DEM shown in Fig. 2b is only necessary to get quantitative elevation values of the structures on the surface.

2.1 Area based matching

The basic problem for an automatic evaluation of stereo images is to find homologue points in the two surface projections of the specimen. That means, that points in the two stereo images have to be identified which are projections of the same object on the specimen. In the field of image processing extensive research has been done to

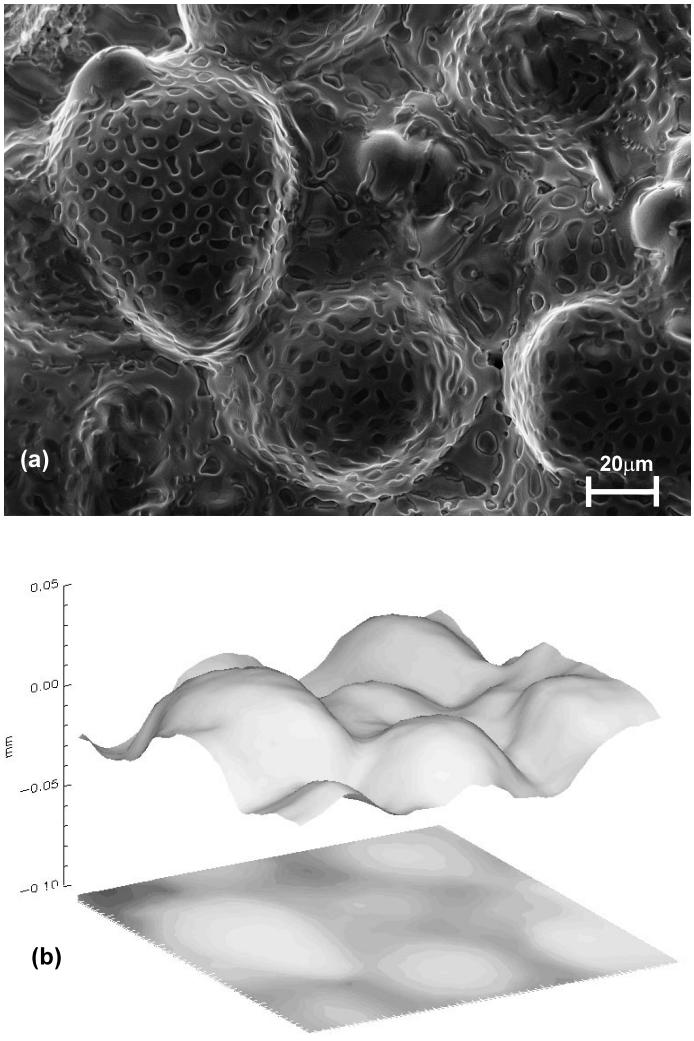

Fig. 2a, b. Monoscopic SEM image **a** of a solder-layer. **b** Shows a shaded surface plot of the 3D-reconstructed object

cope with this problem and the solution procedure is generally called *matching*. Due to the rich contrast and the good signal to noise ratio SEM images are an appropriate basis for an automatic matching procedure.

We decided to adapt and implement an algorithm developed by S. Hensley and S. Shaffer [17]. The basic idea is, given an area $I_1(x, y)$ of an image, to find an area $I_2(x, y)$ in the second image which lies within a certain search area and gives a maximum correlation. Figure 3 demonstrates the problem graphically. By tilting the specimen, the area $I_1(x, y)$ is deformed due to the different projection. The algorithm takes into account such image deformations by using a transformation τ. The transformed area $I_{1,\text{trans}}(x, y) = \tau(I_1(x, y))$ is then correlated with $I_2(x, y)$. The whole algorithm is hierarchical, which means that at the first hierarchical level the image is divided into a small number of rectangles for which initial parallax values are found. At the following levels these rectangles are subdivided and the procedure is repeated. The algorithm is robust against noise and provides subpixel accuracy.

To identify about 10 000 homologue image points a processing time of about three minutes on a UNIX-workstation was needed. The homologue points formed the basis for the 3D surface reconstruction procedure.

2.2 The reconstruction procedure

For the generation of DEMs from the parallaxes we implemented an algorithm first introduced by Piazzesi [18]. Prerequisite for the reconstruction of the topography is the knowledge of the parameters tilt angle, working distance and magnification. Typical tilt angles are 5° to 10°. By solving the Piazzesi equations with the image coordinates $P_{1\,(x,\,y)}$ and $P_{2\,(x,\,y)}$ of homologue points, the three space coordinates can be calculated.

The result of this DEM-generation is shown in Fig. 5 where the DEMs generated from the SEM images in Fig. 4 are shown as shaded surface plot.

The surface reconstruction algorithm is embedded in a larger photogrammetric system XLTT (eXpandable Light Tablett Tool), see [9, 10] for a description. This system offers not only manual point measurements, but also automatic surface reconstruction as well as 3D surface display (using a stereo screen) and measurement of height profiles. Input for XLTT are digital SEM images that were taken on a Leica S440 with a resolution of 1024x768 pixels at 256 gray-levels

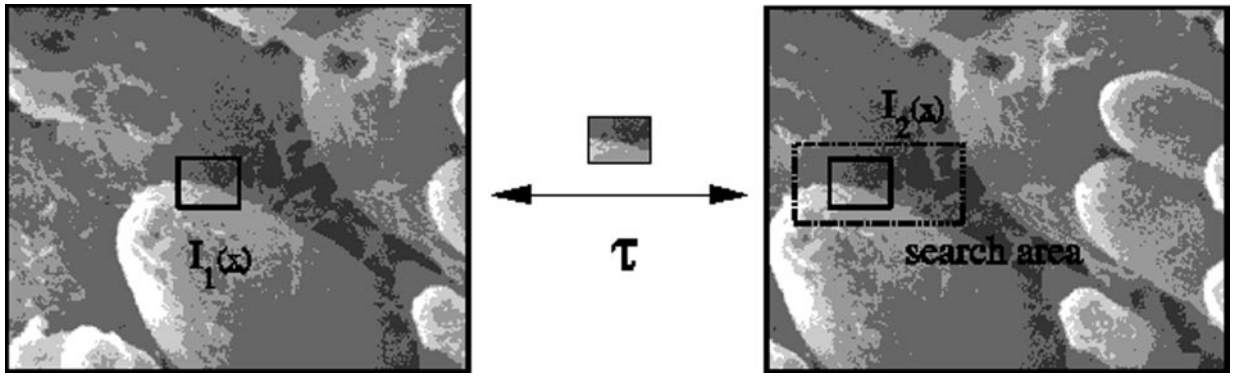

Fig. 3. The parallaxe for an image area I_1 are measured by finding the area I_2 that gives a maximum correlation with I_1

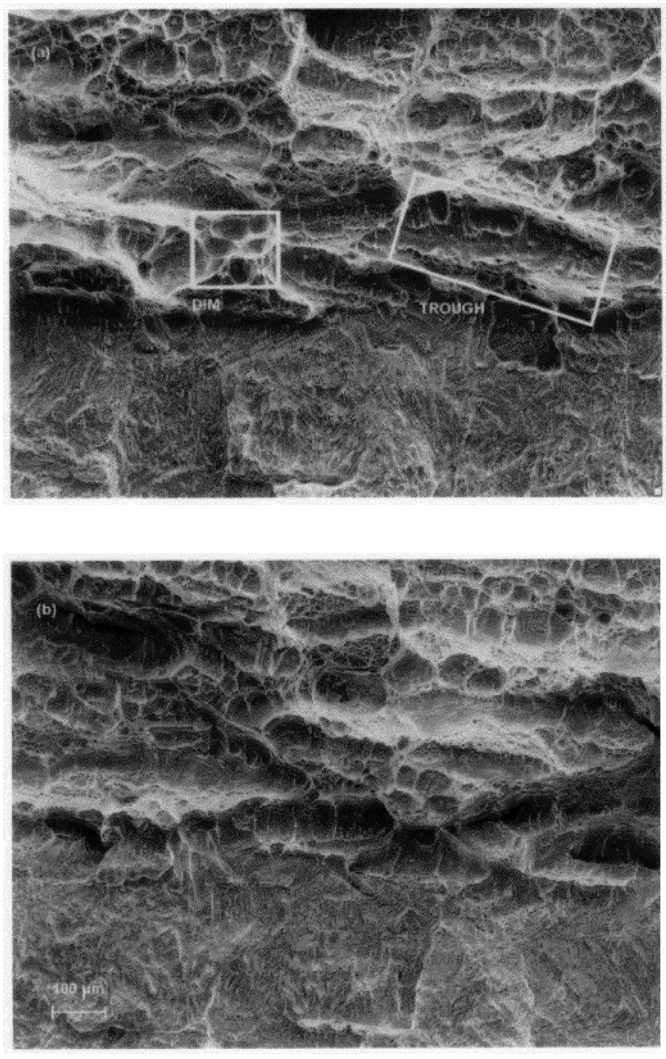

Fig. 4a, b. Red-green anaglyph images of the fracture surface of the specimen half S1 with fatigue crack (*lower half*) and ductile crack (*upper half*). **b** Shows the SEM image of the opposite side S2. Before fracture the *lower left side* of **a** was connected with the *lower right side* of **b**. The investigated material is a solution annealed high strength maraging steel. The images can be viewed with the red-green glasses attached to the page 340 (red glass-left eye).

2.3 Generation of void maps

In fig. 4 the anaglyph images of two fracture surfaces are shown. The investigated material is a solution annealed maraging steel (see later) that was fatigued before cracking it. The two SEM-images were taken at the end of the fatigue crack, that can be seen in the lower half of the two images. In the upper half the typical dimple structure of a ductile fracture surface can be observed. The crack grew from the bottom of the two images to their top. Before the crack separated the two specimen halves, the lower right side of Fig. 4a was connected with the lower left side of Fig. 4b.

The knowledge of one DEM is not sufficient for the evaluation of (5) since the relief of one DEM can be compensated by the relief of the opposite DEM in such a way that the two DEMs fit together perfectly (e.g. cleavage fracture) and no misfit and therefore no plastic

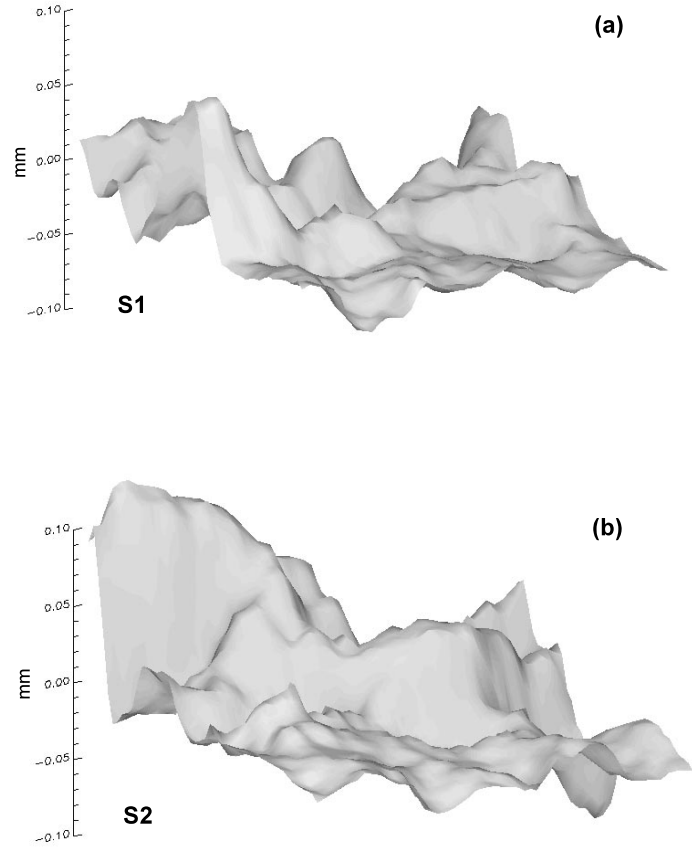

Fig. 5a, b. Digital elevation models (DEMs) of the reconstructed fracture surfaces S1 and S2. The original SEM images are shown in Fig. 4

deformation can be observed. To obtain the extent of plastic deformation a map must be generated which contains the information about the misfit between the two fracture surfaces [19, 20].

Before obtaining a void map, the coupled points on the two specimen halves S1 and S2 have to be identified. For that aim the red-green anaglyph images of the two surfaces were printed on a screen and coupled points on S1 and S2 have been marked. Afterwards the DEMs of S1 and S2 were connected at the proper points. For the used method two points on S1 have to be coupled manually with two points on S2. The coordinate system of S2 has to be translated and rotated in such a way that the two manually identified coupled points on S2 overlap with the two points on S1. From this procedure a translation vector (tr_x, tr_y) and a rotating angle ϕ is obtained. After applying this translation and rotation to the whole DEM of S2, all points of the DEM S1 can be connected with the appropriate coupled points on S2. This method can be applied only when the in-plane deformations on the fracture surface are not too large. Otherwise the rotation angle and translation vector are not the same for all points on the surface. By identifying about 20 manually coupled points we could assure that for the investigated material the in-plane deformations were small enough to allow the use of a single translation and rotation.

In Fig. 6b the result of superimposing S1 and S2 is shown as contour map. The lower half of the image

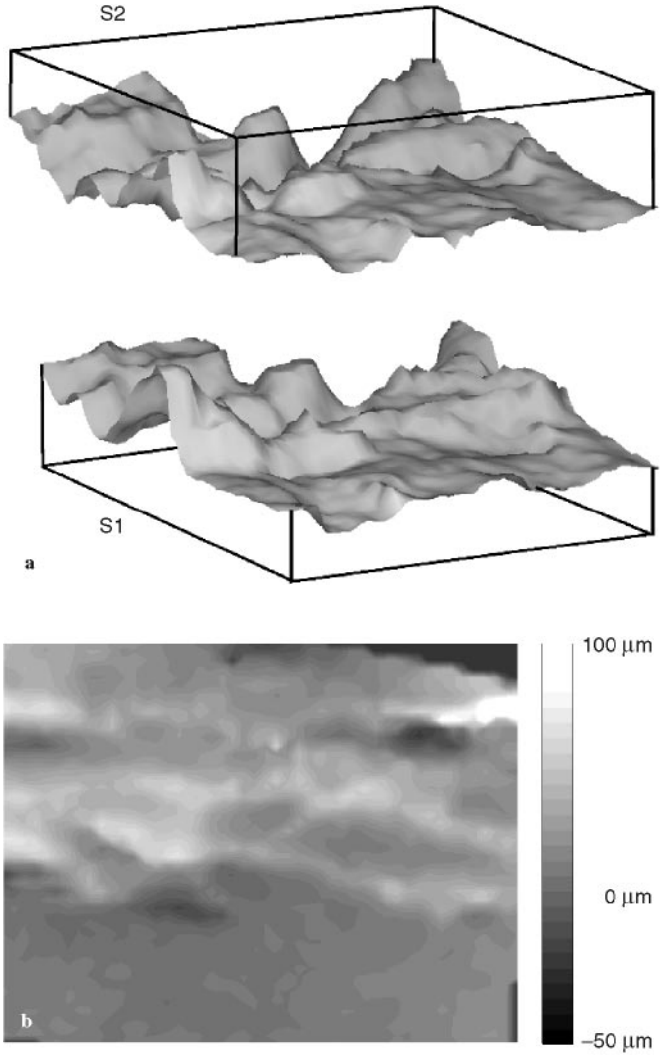

Fig. 6a, b. Void map obtained by superimposing the flipped and rotated DEM of S1 with that of S2 **a**. In **b** a contour-plot of the void map is shown. Each isoline corresponds to a height difference of 5µm. The *left upper corner* in **b** corresponds to the left upper corner in Fig. 4a

corresponds to the fatigue crack where the two surfaces fit together well and the void map shows only little height-differences. The upper half of the image shows an overall elevation relatively to the fatigue crack as well as significant "mountains" and "valleys" due to the misfit between S1 and S2. Dark gray-levels in the contour map mean voids, bright gray levels signify an overlap of the two fracture surfaces.

On the fracture surface we observe dimples of two different scales that are mainly responsible for the misfit. Only a very small contribution is caused by the "classical" dimples as they are marked in the box (DIM) in Fig. 4. Their depth is only a few µm and their contribution to the void energy term in (5) is therefore only very small. The more important contribution is caused by the trough-like deformation whose widths and depths can only be seen in a stereoscopic view. One such trough is marked by the box (TROUGH) in Fig. 4. Their depths, as can be seen in Fig. 6b, vary between 20 µm and 80 µm, therefore their contribution to the void energy is significantly larger than the contribution of the smaller dimples.

The investigated material is an ultra-high-strength maraging steel (Böhler Edelstahl) that was solution annealed for one hour at 820 °C. A yield strength σ_y of 750 MPa and an ultimate tensile strength σ_u of 1050 MPa was measured. With the void map in Fig. 6 and σ_y, (5) can be evaluated. With a hardening exponent of about $n = 0.15$ one can assume an average mean flow stress $\sigma_{amf} \approx 1.3\sigma_u$ [11]. With these parameters a value for the void energy of $D_{void} = 23\ \mathrm{kJ/m^2}$ is obtained.

2.4 Comparison with experiment

Before examining the specimen V720-1 by stereoscopic SEM, a fracture toughness test was done that gave an overall energy dissipation rate $D_{tot} \approx 200\ \mathrm{kJ/m^2}$ for the regime of stationary crack growth. Compared with the value $D_{void} = 23\ \mathrm{kJ/m^2}$ obtained from the analysis of the void map we can conclude that only a *small amount* (in this case about 12 %) of the overall plastic energy is spent in the deformation of the fracture surface. The subsurface small scale yielding that occurs in the plastic zone as well as lateral necking absorbs the remaining part of plastic energy.

In Table 1 the void energy values for three different void maps on specimen V720-1 and for one void map on specimen V720-3 (a side notched CT-specimen of the same material) are given. All values show that only a small amount of the overall dissipated energy is absorbed for the void formation which is in contrast to results presented in [11, 12]. This discrepancy can be explained by the lower yield stress and the higher fracture toughness of the material investigated in this work compared with the materials in [11, 12]. The solution annealed maraging steel V 720 has a large plastic zone. It is therefore probable that deformation processes dissipating plastic energy occur not only in the small process zone around the crack tip (where the voids are formed)but also around this process zone, under the visible fracture surface. The materials investigated in the papers cited above had a higher strength (except the StE47 in [11]) and had therefore a smaller plastic zone. In such a case "subsurface deformations" are less important and most energy must be dissipated in the process zone. For the steel StE47 that has a yield strength comparable to our V 720, Stüwe found no coincidence between the measured fracture toughness and the calculated void energy, probably due to the same reasons mentioned above.

Table 1. Void energy for four different void maps on two specimens

Specimen	Distance from fatigue crack mm	Void-energy kJ/m²
V720-1	0.1	23
	0.1	16
	2.0	19
V720-3	3.0	20

3 Conclusion

- Stereoscopic SEM is a suitable method for the 3D-reconstruction of microscopic objects. The lateral as well as the vertical resolution is limited by the resolution of the SEM only. Since there is no mechanical contact between sensor and object, the method can also be applied to very rough surfaces. Furthermore, stereoscopic SEM images contain, beneath the height information, a lot of image information due to the detailed plastic impression of monoscopic SEM images.
- With digital elevation models of fracture surfaces, generated by automatic image processing, we can reconstruct the plastic deformation and the formation of voids that lead to final fialure. For the estimation of the void energy we take into account the real shape of the specimen and therefore no modelling of the dimple shape is necessary.
- The surfaces show two types of voids: the "classical" dimples with a height and width of several μm and "troughs" that are larger and deeper. The calculation shows that these troughs absorb the main part of the void energy. The comparison with J_{IC} experiments shows that even for the high strength steel examined in this work, the void energy is only a small fraction (about 12%) of the overall plastic energy. The main part of the plastic energy is spent for "subsurface processes" and lateral necking of the specimen.

Acknowledgements. The financial support by the Austrian Fonds zur Förderung der wissenschaftlichen Forschung and by the Österreichische Nationalbankfonds (P10027TEC/FWF 372) is gratefully acknowledged. The authors want to thank Böhler Edelstahl AG for providing the material.

References

1. C.E. Turner: In *Fracture Behaviour and Design of Materials and Structures*, *Proc. of ECF8.* ed. by D. Firrao, (EMAS, U.K. 1990) pp. 933–968
2. C.E. Turner, O. Kolednik: *Fatigue Fracture Eng. Mater. Struct.* **17**, 1089–1107 (1994)
3. A. Boyde: *J. Microsc.* **98**, 452–471 (1973)
4. G.S.Lane: *J. Phys. E* **2**, 565–569 (1969)
5. J.G. Helmcke: *Optik* **12**, 253 (1955)
6. O. Kolednik, H.P. Stüwe: *Eng. Fract. Mech.* **21**, 145–155 (1985)
7. O. Kolednik: *Pract. Metallogr.* **18**, 562–573 (1981)
8. A.J. Krasowsky, V.A. Stepanenko: *Int. J. Fract.* **15**, 203–215 (1979)
9. J. Stampfl, S. Scherer, M. Berchthaler, M. Gruber, O. Kolednik: *Int. J. Fract.* (1996) in print
10. M. Gruber, W. Walcher: In *Spatial Information from Digital Photogrammetry and Computer Vision*, *Int. Arch. Photogramm Remote Sensing* **30**, (3/1), 311–315 (1994)
11. H.P. Stüwe: In *Three Dimensional Constitutive Relations and Ductile Fracture*, ed. by S. Nemat–Nasser (North Holland, Amsterdam 1981) pp. 213–221
12. M.H. Poech, H.F. Fischmeister: *Eng. Fract. Mech.* **43**, 581–588 (1992)
13. ASTM E1152-87, *Annual Book ASTM-Standards* Vol.03.01 (Am. Soc. Test. Mater., Philadelphia PA 1987)
14. H.P. Stüwe: *Eng. Fract. Mech.* **13**, 231–236 (1980)
15. H. Lippmann: *Mechanik des plastischen Fließens* (Springer, Berlin, Heidelberg 1981)
16. R. Hill: *The Mathematical Theory of Plasticity*. (Oxford Univ. Press, Oxford 1971)
17. R.T. Frankot, S. Hensley, S. Shaffer: In *Proc. Int' Geosc. Remote Sensing Symposium 94* (Caltech Pasadena, CA 1994) pp. 1151–1153
18. G. Piazzesi: *J. Phys. E* **6**, 392–396 (1973)
19. H. Miyamoto, M. Kikuchi, T. Kawazoe: *Int. J. Fract.* **42**, 389–404 (1990)
20. N. Ohtsuka, T. Kobayashi, K. Watashi, M. Kikuchi: *Eng. Fract. Mech.* **49**, 859–869 (1994)